Ultrasound vibration measurements based on laser optical feedback imaging

Vadim Girardeau, Olivier Jacquin, Olivier Hugon, Eric Lacot

Ultrasound vibration measurements based on Laser Optical Feedback Imaging (LOFI)

VADIM GIRARDEAU,[1] OLIVIER JACQUIN,[1] OLIVIER HUGON,[1] ERIC LACOT[1,*]

[1]Univ. Grenoble Alpes, CNRS, LIPhy, F-38000 Grenoble, France
*Corresponding author: eric.lacot@univ-grenoble-alpes.fr

This paper is devoted to the detection of ultrasound vibrations with nanometric amplitude by using a LOFI (Laser Optical Feedback Imaging) setup. By means of numerical simulations, we show typical examples of ultrasound vibrations having different temporal shapes (harmonic and transient) extracted from the laser output power modulation induced by the frequency shifted optical feedback. Considering the laser quantum noise dynamic and the detection noise separately, we show that the simulated vibration noise is in good agreement with the theoretical prediction. Also, we demonstrate that Ultra High Frequencies (in the GHz range) can be detected by using a usual LOFI setup with a low power laser (few mW) and a conventional detection with a usual white noise level. Then we show how the noise of a short transient vibration can be reduced by the reconstruction of its wide vibration spectrum by concatenation. Finally, the experimental detection of transient-harmonics ultrasound vibrations propagating in water and detected at the air/water interface is presented.© 2018 Optical Society of America

1. INTRODUCTION

Laser properties (e.g. power, polarization, coherence, dynamical behavior) can be significantly affected and modified by optical feedback [1,2] that allows for the realization of non-conventional sensors. One potential application is Laser Feedback Interferometry (LFI), where the steady-state intensity of a laser is modified by coherent optical feedback from an external target. This technique is sensitive to the phase (distance and motion of the target [3]) and the signal depends on the reflectivity of the target. However, when the amount of re-injected light is very small, the interference contrast occurring inside the laser cavity is drastically reduced. To overcome this problem, one solution is to use the dynamical properties of the laser, which can be several orders of magnitude more sensitive to optical feedback than the laser steady-state properties. The maximum of the modulation is obtained when the frequency shift is resonant with the laser relaxation oscillation frequency. In this condition, an optical feedback level as low as -170 dB (i.e. 10^{17} times weaker than the laser intra-cavity power) has been detected [4]. Since the pioneering work of K. Otsuka on self-mixing modulation effect in a class-B laser [5], the dynamical sensitivity of lasers to frequency shifted optical feedback has been used in metrology [6,7], for example in self mixing Laser Doppler Velocimetry (LDV) [4,8,9], in vibrometry [10-12] and in Laser Optical Feedback Imaging (LOFI) [13-15]. Compared to conventional optical heterodyne detection, a LOFI setup allows for higher (several order of magnitude) signal to noise ratio when working with a low power laser (a few mW) and a conventional detection with a usual noise level [16-18].

The main objective of the present paper is to demonstrate the possibility to accurately measure very small vibration amplitudes (in the nanometer range) in the ultrasound domain (in the MHz range) by using a LOFI setup with a relatively low power laser (tens of mW). Even if nanometer measurements based on SMI (Self Mixing Interferometry) have already been realized, either for acoustic perturbations or for nm-sized vibrations [19-20], the use of a LOFI setup is motivated by the combination of the four following reasons: i) The LOFI interferometer is always self-aligned because the laser simultaneously fulfils the functions of the source (i.e. photons-emitter) and of the photo-detector (i.e. photons-receptor); ii) The phase of the LOFI beating is sensitive to the round-trip phase shift between the laser and the vibrating target. iii) The LOFI sensitivity allows to analyse targets from which the back-reflected (or back-scattered) electric field is very weak. iv) The LOFI detection is shot noise limited (even with a low power laser and a conventional detection) in a frequency range located near the relaxation oscillation frequency of the laser [17-18].

This article is organized as follows. In section 2, we firstly recall the equations governing the dynamics of a laser with a frequency-shifted optical reinjection back-scattered from a vibrating target. Secondly a conventional LOFI setup is described. The next section (section III) is devoted to the detection of ultrasound vibrations. The signal processing to extract vibration measurements from the laser modulation is explained and we show typical examples of numerical vibration signals (harmonic and transient) extracted from the laser dynamic. Considering the laser quantum noise and also the detection noise, we determine the maximum vibration frequency that can be detected by using a LOFI setup. The end of section 3 is devoted to the experimental measurement with a LOFI setup of transient-harmonics

ultrasound vibrations propagating in water and detected at the air/water interface. The final section (section 4) is a general discussion of these results and to their prospective applications, principally for Photo-Acoustic (PA) imaging.

2. LASER OPTICAL FEEDBACK IMAGING (LOFI) FOR VIBROMETRY

A. Basic equations of the laser dynamics

For an optical feedback characterized by a weak power reflectivity ($R_e \ll 1$) and an optical frequency shift (F_e), the dynamical behavior of the laser can be described by the following set of differential equations [17]:

$$\frac{dI(t)}{dt} = BI(t)D(t) - \gamma_c I(t)$$
$$+ \gamma_c 2\sqrt{R_e} I(t) \cos\left[\Omega_e t + \Phi_e(t)\right] + F_I(t) \qquad \textbf{(1a)}$$

$$\frac{dD(t)}{dt} = \gamma_1 \left[D_0 - D(t)\right] - BI(t)D(t) + F_D(t) \qquad \textbf{(1b)}$$

where I and D are respectively the laser intensity (photon unit) and the population inversion (atom unit). γ_1 is the decay rate of the population inversion, γ_c is the laser cavity decay rate, $\gamma_1 D_0$ is the pumping rate and B is the Einstein coefficient related to the laser transition cross section. In this modeling, the laser output power (photons/s unit) and the intra-cavity laser intensity (photon unit) are linked through the equation: $P_{out}(t) = \gamma_c I(t)$. Regarding the noise, the laser quantum fluctuations are principally described by the Langevin noise functions $F_I(t)$ and $F_D(t)$, which have a zero mean value and a white noise type correlation function [21,22].

In Eq. (1a), the harmonic modulation expresses the coherent interaction (i.e. the beating at the angular frequency: $\Omega_e = 2\pi F_e$) between the lasing and the feedback electric field. The optical light back-reflected (or back-scattered) by a target is characterized by the effective power reflectivity R_e (taking into account the albedo of the target under investigation, the efficiency of the frequency shifter, the optical losses between the laser and the target and also the overlapping between the feedback electric field and the intra-cavity laser mode). For a vibrating target, the optical feedback is also characterized by the time dependent optical phase shift:

$$\Phi_e(t) = \Phi_0 + \Phi_a(t) = \frac{2\pi}{\lambda_c} 2\left[d_0 + d_a(t)\right], \quad \text{induced by the}$$

distance between the laser and the target, where λ_c is the laser wavelength, while d_0 and $d_a(t) \ll \lambda_c$ are respectively the mean distance between the laser and the target and the small target displacement induced by the vibration. Without loss of generality, we supposed that: $\Phi_0 = m \times 2\pi$.

The use of Eqs. (1) supposes that the round trip time between the laser and the target is short compared to the modulation period ($\tau_e \approx 2d_0/c \ll 1/F_e$) and therefore that the time-shift of the intensity feedback can be neglected ($I(t - \tau_e) \approx I(t)$).

In the absence of optical feedback ($R_e = 0$), the laser steady-state is given by:

$$D_S = \frac{\gamma_c}{B}, \qquad \textbf{(2a)}$$

$$\langle P_{out} \rangle = \gamma_c I_S = \gamma_c I_{sat}\left[\eta - 1\right], \qquad \textbf{(2b)}$$

where $\eta = \dfrac{D_0}{D_S}$ is the normalized pumping parameter and $I_{sat} = \dfrac{\gamma_1}{B}$ is related to the saturation intensity of the laser transition.

Also, for $R_e = 0$, the intrinsic dynamics of a class-B laser ($\gamma_c \gg \gamma_1 \eta$) is characterized by damped relaxation oscillations of the laser output power with a relaxation angular frequency $\Omega_R = \sqrt{\gamma_1 \gamma_c (\eta - 1)}$ and a damping rate $\Delta\Omega_R = \gamma_1 \eta/2$. This transient dynamics allows to determine the modulation transfer function of the laser dynamics (also called the LOFI gain):

$$G_R(\Omega) = \frac{\gamma_c (i\Omega + \Delta\Omega_R)}{\Omega_R^2 - \Omega^2 + i\Omega \times \Delta\Omega_R},$$
$$= \left|G_R(\Omega)\right| \exp\left[i\Phi_R(\Omega)\right] \qquad \textbf{(3)}$$

In a real system, the transient dynamics is constantly stimulated by the laser quantum noise described by the Langevin forces $F_I(t)$ and $F_D(t)$.

For a laser with frequency shifted optical feedback ($R_e \neq 0$) and for a weak modulation contrast of the laser intensity ($2\sqrt{R_e}\left|G_R(\Omega_e)\right| \ll 1$), the laser dynamics is linear and the output power modulation of the laser is given by the convolution product ($\otimes$ symbol) between the beating modulation at the carrier frequency and the impulse response of the laser dynamics [i.e. the inverse Fourier Transform (FT^{-1}) of the modulation transfer function $G_R(\Omega)$]:

$$\Delta P_{out}(t) = P_{out}(t) - \langle P_{out} \rangle$$
$$= 2\sqrt{R_e} \langle P_{out} \rangle \begin{bmatrix} FT^{-1}\left[G_R(\Omega)\right] \otimes \\ \exp\left[i\left(\Omega_e t + \Phi_a(t)\right)\right] \\ +cc \end{bmatrix}, \qquad \textbf{(4)}$$

where " cc " stands for complex conjugate.

B. Experimental setup

To measure the ultrasound vibration of a target (i.e. to determine $\Phi_a(t)$), we have used a LOFI setup. A schematic diagram of this setup is shown in Fig. 1. The laser is a diode pumped Nd:YAG microchip laser. The maximum available pump power is 400 mW at 810 nm, giving a 50 mW output power at a central wavelength of $\lambda_c = 1064\,nm$ for the microchip laser. It has a plane-parallel cavity, which is stabilized by the thermal lens induced by the Gaussian pump beam. The two dielectric mirrors are directly coated on the laser material (full cavity). The input dichroic mirror transmits the pump power and totally reflects the infrared laser wavelength. On the other side, the dichroic output mirror allows to totally reflect the pump power (to increase the pump power absorption and therefore the laser

efficiency) and only partially reflects (95%) the laser wavelength. The microchip has a relatively short cavity $L_c \approx 1\,mm$, which ensures a high cavity damping rate (γ_c) and therefore a good sensitivity to optical feedback.
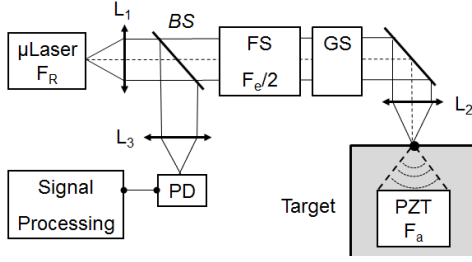

Fig. 1. Schematic diagram of the LOFI setup for vibrometry. µLaser: microchip laser with a relaxation oscillations frequency F_R. L₁, L₂ and L₃: Lenses, BS: Beam Splitter, PD: Photodiode, FS Frequency Shifter with a round trip frequency-shift F_e GS: Galvanometric Scanner, PZT: Piezo Electric Transducer with a vibration frequency F_a. The transducer is immerged inside a tank fill with water and the acoustic wave is focused on the air/water interface in order to generate surface measurable perturbations of the surface of the fluid

Part of the light diffracted and/or scattered by the vibrating target returns inside the laser cavity after a second pass through the frequency shifter. Therefore, the optical frequencies of the reinjected light are shifted by F_e. This frequency shift can be adjusted and is typically of the order of the laser relaxation frequency F_R, which is in the megahertz range for the microchip laser used here. Finally, the coherent interaction (beating) between the lasing electric field and the frequency-shifted reinjected field leads to a modulation of the laser output power. For detection purposes, a small part of the laser output beam is sent to reversed biased PIN photodiode (THORLABS/DET110). The delivered voltage is send to DAQ card (SPECTRUM/ M3I.4111) and processed by a PC to finally obtain quantitative vibration measurements.

One can notice that even if the LOFI setup is usually used to obtain images pixel by pixel with a raster scan, only punctual measurements have been made in the present work. Also, one can notice that in comparison with a conventional heterodyne interferometer, the LOFI setup shown here does not require complex alignment. Indeed, the LOFI interferometer is always self-aligned because the laser simultaneously fulfils the functions of the source (i.e. photons-emitter) and the photo-detector (i.e. photons-receptor).

Experimentally, to generate vibrations (i.e. a time dependant phase $\Phi_a(t)$), an ultrasound transducer (NDT Systems, IBMF104) having a central frequency of $F_a = 10\,MHz$ and a band-pass of several MHz has been used. The transducer, with a diameter of 13 mm and a focal length of 26 mm, is immerged inside a tank filled with water and the depth of the transducer is aligned in that way, that its focus lays near to the air/water interface in order to generate measurable perturbations in the surface of the fluid.

3. ULTRASOUND LOFI VIBROMETRY

To demonstrate how different kinds of vibrations (i.e. $\Phi_a(t)$) can be extracted from the laser modulation [i.e. from Eq. (4)] induced by a frequency shifted optical feedback, we have numerically solved the set of differential equations given by Eqs. (1) with the following

parameters for the laser and the detection, which correspond to typical experimental conditions when working with a LOFI setup [17,18]:

$$P_{out} = 3 \times 10^{17}\ photons/s\ ,\ \eta = 1.2\ ,\ \lambda_c = 1064\,nm\ , \quad \textbf{(5a)}$$

$$F_R \approx 1.1\,MHz\ ,\ \gamma_c = 5 \times 10^9\ s^{-1}\ ,\ \gamma_1 = 5 \times 10^4\ s^{-1}\ ; \quad \textbf{(5b)}$$

$$\frac{\left|\overset{)}{N}_D\right|}{\sqrt{\Delta F}} = \frac{8 \times 10^{-8}\ \dfrac{W}{\sqrt{Hz}}}{hc/\lambda_c}\ ;\ \Delta F = 8\,kHz\ ; \quad \textbf{(5c)}$$

$$\frac{\left|\overset{)}{N}_{SN}\right|}{\sqrt{\Delta F}} = \frac{1.4 \times 10^{-10}\ \dfrac{W}{\sqrt{Hz}}}{hc/\lambda_c}\ ;\ \left|\overset{)}{N}_Q(\Omega)\right| = \left|G_R(\Omega)\right|\left|\overset{)}{N}_{SN}\right|\ ;\ \textbf{(5d)}$$

In Eq. (5c), $\left|\overset{)}{N}_D\right|$ and $\left|\overset{)}{N}_{SN}\right|$ are respectively the detection noise and the shot noise (both in photon unit) for a detection bandwidth ΔF (i.e. a signal acquisition time T). h is the Plank constant and c is the speed of light. Eq. (5d) gives the relationship between the shot noise and the laser quantum noise $\left|\overset{)}{N}_Q(\Omega)\right|$ when the dynamical amplification by the LOFI gain is taken into account.

To clearly identify the contributions of the laser quantum noise and of the detector noise on the vibration measurements, our study is made in two steps. Firstly, the effect of the laser quantum noise is analyzed alone ($\left|\overset{)}{N}_Q(\Omega)\right| \neq 0$ and $\left|\overset{)}{N}_D(\Omega)\right| = 0$) and secondly, the detector noise is also taken into account ($\left|\overset{)}{N}_Q(\Omega)\right| \neq 0$ and $\left|\overset{)}{N}_D(\Omega)\right| \neq 0$).

A. Numerical study of harmonic vibrations
Fig. 2 shows a typical power spectrum of the laser dynamic when the laser is subjected to a weak optical feedback ($F_e = 5.4 \times F_R$ and $R_e = 10^{-7}$) carrying the information of a harmonic vibration of the target:

$$\Phi_a(t) = \frac{2\pi}{\lambda_c} 2d_a(t) = \hat{\Phi}_a \times \sin(\Omega_a t + \varphi_a)\ , \quad \textbf{(6)}$$

with a small vibration amplitude ($\hat{\Phi}_a = 2\pi/50$, i.e. $\hat{d}_a = \lambda_c/100 \approx 10\,nm$), an acoustic frequency of several megahertz ($F_a = \Omega_a/2\pi = 4.3 \times F_R$) and φ_a an additional phase shift arbitrarily chosen equal to: $\varphi_a = 2\pi/3$. By using Eq. (4), this vibration leads to a laser output power modulation given by :

$$\Delta P_{out}(t) =$$

$$2\sqrt{R_e}\left\langle P_{out}\right\rangle \left\{ \begin{aligned} &\sum_{n=-\infty}^{n=+\infty} J_n(\hat{\Phi}_a)\left|G_R(\Omega_e + n\Omega_a)\right| \times \\ &\cos\left[(\Omega_e + n\Omega_a)t + n\varphi_a + \Phi_R(\Omega_e + n\Omega_a)\right] \end{aligned} \right\} \quad \textbf{(7)}$$

where $J_n(\Phi_a)$ is the Bessel function of the first kind and of order n. For a small vibration amplitude ($\hat{\Phi}_a \ll 2\pi$) the sum over the Bessel functions reduces to only the following three terms:

$$J_0\left(\hat{\Phi}_a\right) \approx 1 , \quad J_{+1}\left(\hat{\Phi}_a\right) = -J_{-1}\left(\hat{\Phi}_a\right) \approx \hat{\Phi}_a/2 , \qquad \textbf{(8a)}$$

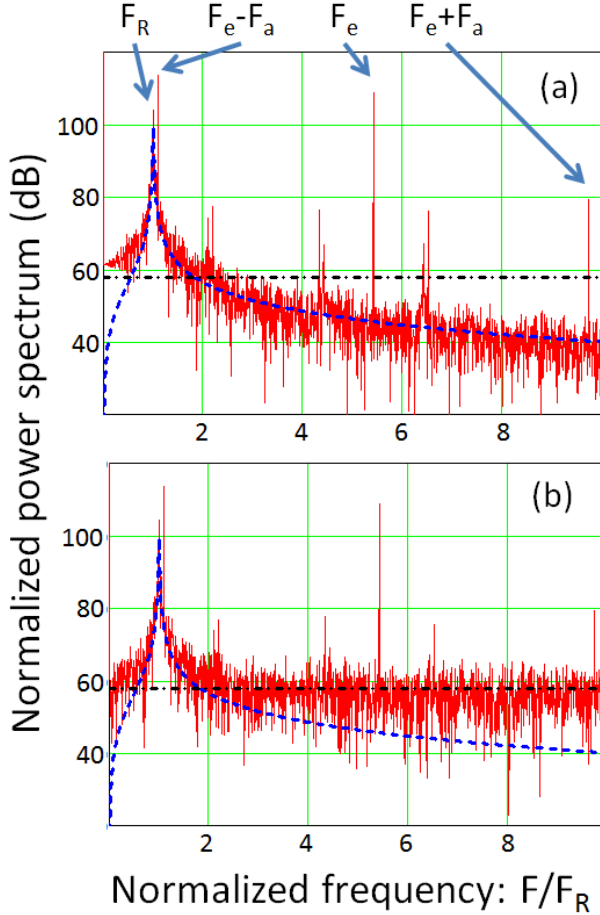$$J_n\left(\hat{\Phi}_a\right) \approx 0 \quad |n| \geq 2 . \qquad \textbf{(8b)}$$

Fig. 2. Numerical simulations. Normalized power spectrum of the laser intensity dynamics. The normalization is made with the shot-noise. a) With the laser quantum noise alone. b) With the laser quantum noise and the detection noise. The dashed curve is a fit of the laser quantum noise power spectrum. The horizontal dashed-dotted line is the mean value of the detection noise power spectrum. Optical feedback: $R_e = 10^{-7}$, $F_e = 5.4 \times F_R$. Harmonic vibration: $\hat{\Phi}_a = 2\pi/50$, $\varphi_a = 2\pi/3$ $F_a = 4.3 \times F_R$ ($F_e - F_a = 1.1 \times F_R$). The laser and detection parameters are given in Eqs. (5a-d).

In Figs. 2(a) and 2(b), the beating signal is therefore principally composed of one peak at the carrier frequency (F_e) and of the two vibration sidebands ($F_e \pm F_a$). In Fig. 2(a), the noise corresponds to the dynamically amplified laser quantum noise, which presents a resonance at the laser relaxation oscillation frequency F_R. Even if the feedback level is low ($R_e = 10^{-7}$), the modulation contrast of the laser output power is relatively high ($2\sqrt{R_e}\left|G\left(\Omega_e\right)\right| = 0.56$) and one can also observe smaller peaks induced by the non-linear laser dynamics, at sum and difference frequencies: $F_e \pm \left(F_e - F_a\right), F_e \pm F_R, \ldots$

Eqs. (7-8) shows that the parameters of a harmonic vibration ($\hat{\Phi}_a$ and φ_a) can be simply determined from the Fourier spectrum by doing the ratio between the rectified amplitudes of the complex peaks at the carrier frequency and at the side-band frequencies:

$$-\hat{\Phi}_a \exp\left(-j\varphi_a\right) \approx 2 \frac{\overset{}{I}\left(\Omega_e - \Omega_a\right)/G\left(\Omega_e - \Omega_a\right)}{\overset{}{I}\left(\Omega_e\right)/G\left(\Omega_e\right)} , \qquad \textbf{(9a)}$$

$$\hat{\Phi}_a \exp\left(+j\varphi_a\right) \approx 2 \frac{\overset{}{I}\left(\Omega_e + \Omega_a\right)/G\left(\Omega_e + \Omega_a\right)}{\overset{}{I}\left(\Omega_e\right)/G\left(\Omega_e\right)} , \qquad \textbf{(9b)}$$

with $\overset{}{I}\left(\Omega\right) = FT\left[\Delta P_{out}\left(t\right)\right]$, where "$FT$" stands for Fourier Transform.

Due to the assumption $J_0\left(\hat{\Phi}_a\right) \approx 1$, the spectrum of Fig. 2(a) allows us to remind what is usually called the signal to noise ratio (SNR) of the LOFI modulation [17] :

$$SNR_{LOFI} = \sqrt{2} \frac{\left|\overset{}{I}\left(\Omega_e\right)\right|}{\left|\overset{}{N}_Q\left(\Omega_e\right)\right|} = \frac{\sqrt{2}\sqrt{R_e}P_{out}\left|G_R\left(\Omega_e\right)\right|}{\sqrt{P_{out}}\sqrt{2}\left|G_R\left(\Omega_e\right)\right|\sqrt{\Delta F}}$$
$$= \frac{\sqrt{R_e P_{out}}}{\sqrt{\Delta F}} \qquad \textbf{, (10)}$$

where in the Fourier domain, $\left|\overset{}{I}\left(\Omega_e\right)\right|$ and $\left|\overset{}{N}_Q\left(\Omega_e\right)\right|$ are respectively, the height of the peak at the modulation frequency Ω_e and the amount of laser quantum noise in the detection bandwidth ΔF around this frequency. In Eq. (10) the multiplicative number $\sqrt{2}$ comes from the fact that the LOFI signal is usually obtained by using both the positive ($+\Omega_e$) and the negative ($-\Omega_e$) modulation frequencies of the Fourier spectrum.

Since the LOFI signal and the laser quantum noise have the same amplification gain, the last part of Eq. (10) shows that the LOFI SNR is independent of the frequency shift Ω_e. Eq. (10) also shows that the LOFI detection is shot-noise limited when the detection is limited by the amplified laser quantum noise [17]. Indeed, with Eq. (10), one obtains $SNR_{LOFI} = 1$, when only one photon is reinjected inside the laser cavity during the detection integration time. In the example of Fig. 2(a), the LOFI SNR is roughly equal to : $SNR_{LOFI} \approx 2 \times 10^3$ (i.e. $66\,dB$) in agreement with the theoretical prediction given by Eq. (10) for an effective feedback reflectivity of $R_e = 10^{-7}$. We will show farther in this paper how the vibration amplitude noise $\Delta\hat{\Phi}_a$ (or equivalently $\Delta\hat{d}_a = \frac{\lambda}{2}\frac{\Delta\hat{\Phi}_a}{2\pi}$) and the vibration phase noise $\Delta\varphi_a$ can be expressed simply from the LOFI SNR given by Eq. (10).

In Fig. 2(b), the LOFI signal is the same, but now the noise is composed of the sum of the resonant laser quantum noise and of the detection noise, which is an additive white noise with a flat spectrum. In the example of Fig. 2(b), one can observe that the resonant laser quantum

noise is higher than the detection noise in a frequency range roughly given by: $0.5 \leq F/F_R \leq 2$. Therefore the LOFI detection is shot-noise limited only in this range located in the vicinity of the relaxation oscillation frequency [17].

Also, the comparison of Figs. 2(a) and 2(b) shows that the SNR of the lower vibration side-band ($F_e - F_a$), which is located near the relaxation frequency is the same with an without the detector noise, while the SNR of the upper vibration side-band ($F_e + F_a$), which is far away the relaxation frequency, is reduced by the detector noise, which is the dominant noise at this frequency. In a real experimental situation where the detector noise exists, we therefore used Eq. (9a) [instead of Eq. (9b)] to determine the vibration parameters with the lowest noise.
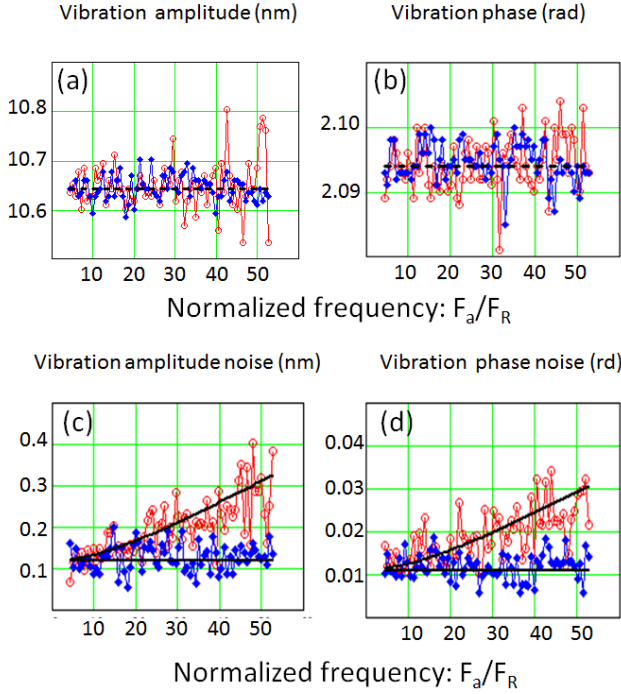

Fig. 3. Numerical simulations. Detection of a harmonic vibration with an amplitude $\hat{\Phi}_a = 2\pi/50$ (i.e. $\hat{d}_a = 1064\,nm/100 = 10.64\,nm$) and a phase shift $\varphi_a = 2\pi/3 = 2.094\,rad$, for an increasing value of the acoustic frequency F_a. Optical feedback: $R_e = 10^{-7}$, $F_e - F_a = 1.1 \times F_R$. Left column (a,c) measured signal ($\hat{d}_a = \dfrac{\hat{\Phi}_a}{2\pi}\dfrac{\lambda_c}{2}$) and noise ($\Delta\hat{d}_a$) of the vibration amplitude. Right column (b,d), measured signal (φ_a) and noise ($\Delta\varphi_a$) of the vibration phase shift. Diamonds: measurements made when only the laser quantum noise is taken into account. Circles: measurements made with both the detector noise and the laser quantum noise. Horizontal dashed line: mean value of the signal. Full lines: theoretical predictions of the vibration noises given by Eqs. (13, 14) and (17). The laser and detection parameters are given in Eqs. (5a-d).

Fig. 3 shows the extraction of the vibration amplitude $\hat{\Phi}_a$ and of the vibration phase φ_a obtained [by using Eq. (9a)] for different values of the angular acoustic frequency Ω_a, with the imposed constraint that

the lower side-band is always at the same position near the relaxation frequency: $\Omega_e - \Omega_a = 1.1 \times \Omega_R$ Under this constraint, the lower side band is always shot noise limited and an increase of the acoustic frequency (Ω_a) is always linked with the same increase of the carrier frequency (Ω_e).

To determine the vibration noises $\Delta\hat{d}_a = \left(\lambda\Delta\hat{\Phi}_a\right)/4\pi$ and $\Delta\varphi_a$, the measurements are made ten times for each acoustic frequency and the standard deviations are calculated, while an average $\langle\ \rangle$ is made to obtain the vibration parameters ($\langle\hat{d}_a\rangle$ and $\langle\varphi_a\rangle$).

Figs. 3(a) and 3(b) clearly show a good agreement between the values extracted from the numerical simulations and the exact values for both the vibration amplitude $\hat{d}_a$ and of the vibration phase φ_a. Figs. 3(c) and 3(d) show the vibration noises ($\Delta\hat{d}_a$ and $\Delta\varphi_a$) obtained with and without the detector noise (i.e. when the detector noise is added or not to the amplified laser quantum noise). One can observe that the vibration noises are frequency independent when only the laser quantum noise is taken into account, while it increases when the detection noise is added.

Without the detector noise, (i.e. when only the laser quantum noise is taken into account in the numerical simulation), Eq. (9a) allows calculating the relative noise of the amplitude of a harmonic vibration (subscript h) in the quantum shot-noise limit (subscript Q):

$$\frac{\Delta\hat{\Phi}_{a,h,Q}}{\hat{\Phi}_a} = \sqrt{\left(\frac{\left|\overset{\backsim}{N}_Q\left(\Omega_e - \Omega_a\right)\right|}{\left|\overset{\backsim}{I}\left(\Omega_e - \Omega_a\right)\right|}\right)^2 + \left(\frac{\left|\overset{\backsim}{N}_Q\left(\Omega_e\right)\right|}{\left|\overset{\backsim}{I}\left(\Omega_e\right)\right|}\right)^2}\,,$$
$$\approx \frac{\left|\overset{\backsim}{N}_Q\left(\Omega_e - \Omega_a\right)\right|}{\left|\overset{\backsim}{I}\left(\Omega_e - \Omega_a\right)\right|} \qquad \textbf{(11)}$$

In the case of a small vibration amplitude, Fig.2(a) shows that the relative noise at the carrier frequency is at least 2 orders of magnitude lower than the relative noise of the lower side-band frequency. This observation justifies the approximation that is made in the last part of Eq. (11).

Remembering that the noise amplitude is proportional to the laser dynamic gain [see Eq. (5d)] one obtains:

$$\left|\overset{\backsim}{N}_Q\left(\Omega_e - \Omega_a\right)\right| = \left|\overset{\backsim}{N}_Q\left(\Omega_e\right)\right|\left|G\left(\Omega_e - \Omega_a\right)\right|/\left|G\left(\Omega_e\right)\right|, \qquad \textbf{(12)}$$

and finally, by using Eqs. (9-12):

$$\Delta\hat{\Phi}_{a,h,Q} \approx 2\frac{\left|\overset{\backsim}{N}_Q\left(\Omega_e\right)\right|}{\left|\overset{\backsim}{I}\left(\Omega_e\right)\right|} = 2\frac{\sqrt{2}}{SNR_{LOFI}} = 2\frac{\sqrt{2\Delta F}}{\sqrt{R_e P_{out}}}. \qquad \textbf{(13)}$$

Also, as already explained in the appendix of [23], the measured amplitude and phase noises of a modulation with an additive white noise are linked through the following equations:

$$\Delta\varphi_{a,h,Q} \approx \frac{\Delta\hat{\Phi}_{a,h,Q}}{\hat{\Phi}_a}. \qquad \textbf{(14)}$$

In agreement with the theoretical prediction given by Eq. (13) and (14), the numerical simulations shown in Figs. 3(c) and 3(d) show that the noises on the vibration amplitude and phase are frequency independent when the LOFI detection is limited by the amplified laser

quantum noise. More precisely, with: $SNR_{LOFI} \approx 2 \times 10^3$, $\hat{\Phi}_a = 2\pi/50$ (i.e. $\hat{d}_a = \lambda_c/100 \approx 10\,nm$) and $\varphi_a = 2\pi/3 = 2.094\,rad$, one obtains: $\Delta\hat{\Phi}_{a,h,Q} = 1.4 \times 10^{-3}\,rad$ (i.e. $\Delta\hat{d}_{a,h,Q} = 0.12\,nm$) and $\Delta\varphi_{a,h,Q} = 1.1 \times 10^{-2}\,rad$.

When the detector noise (which is frequency independent) is added, Fig 2(b) shows that the power spectrum of the detection noise is flat. If $\overset{\rangle}{N}_D$ is the amount of detector noise in the detection bandwidth ΔF [see Eq. (5c)], one can see that the noise on the vibration sideband is always given by the laser quantum noise ($\left|\overset{\rangle}{N}_Q\left(\Omega_e - \Omega_a\right)\right| >> \left|\overset{\rangle}{N}_D\right|$), while the noise at the carrier frequency is now dominated by the detector noise ($\left|\overset{\rangle}{N}_D\right| >> \left|\overset{\rangle}{N}_Q\left(\Omega_e\right)\right|$). Under these typical conditions, Eq. (11) becomes:

$$\frac{\Delta\hat{\Phi}_{a,h}}{\hat{\Phi}_a} \approx \sqrt{\left(\frac{\left|\overset{\rangle}{N}_Q\left(\Omega_e - \Omega_a\right)\right|}{\left|\overset{\rangle}{I}\left(\Omega_e - \Omega_a\right)\right|}\right)^2 + \left(\frac{\left|\overset{\rangle}{N}_D\right|}{\left|\overset{\rangle}{I}\left(\Omega_e\right)\right|}\right)^2}$$

$$\approx \sqrt{\left(\frac{\Delta\hat{\Phi}_{a,h,Q}}{\hat{\Phi}_a}\right)^2 + \left(\frac{\Delta\hat{\Phi}_{a,h,D}}{\hat{\Phi}_a}\right)^2} \quad \textbf{(15)}$$

Eqs. (11 and 15) allows to define the contribution of the detector noise (subscript D) in the measured amplitude noise of a harmonic vibration (subscript h):

$$\Delta\hat{\Phi}_{a,h,D} \approx \hat{\Phi}_a \frac{\left|\overset{\rangle}{N}_D\right|}{\left|\overset{\rangle}{I}\left(\Omega_e\right)\right|} \approx \hat{\Phi}_a \frac{\left|\overset{\rangle}{N}_D\right|}{\left|\overset{\rangle}{N}_Q\left(\Omega_e\right)\right|} \frac{\sqrt{2}}{SNR_{LOFI}}. \quad \textbf{(16)}$$

Finally, by combining Eqs. (13a) and (16), one obtains the noise on the vibration components:

$$\Delta\hat{\Phi}_{a,h} = \sqrt{\Delta\hat{\Phi}_{a,h,Q}^2 + \Delta\hat{\Phi}_{a,h,D}^2}$$

$$= \frac{2\sqrt{2}}{SNR_{LOFI}} \left[1 + \left(\frac{\hat{\Phi}_a}{2} \frac{\left|\overset{\rangle}{N}_D\right|}{\left|\overset{\rangle}{N}_Q\left(\Omega_e\right)\right|}\right)^2\right]^{\frac{1}{2}} \quad \textbf{(17a)}$$

$$\Delta\varphi_{a,h} \approx \frac{\Delta\hat{\Phi}_{a,h}}{\hat{\Phi}_a} \quad \textbf{(17b)}$$

When the LOFI detection is limited by the detector noise, Figs. 3(c) and 3(d) show in agreement with the theoretical prediction given by Eqs. (17a-b) an increase of the noise on the vibration amplitude and phase when the acoustic frequency increases (i.e. when the carrier frequency increases through the constraint: $\Omega_e = \Omega_a + 1.1 \times \Omega_R$). This increase of the noise comes from the fact that the peak at the carrier frequency drowns more and more in the detector noise spectrum as the carrier frequency increases.

Also, Eq. (17a) allows to determine the maximum possible value of the acoustic frequency $\Omega_{a,\max}$ that can be detected by using a LOFI setup, for a given detector noise level. Indeed, far away from the resonance ($\Omega_{e,\max} - \Omega_R >> \Delta\Omega_R$), the condition $\Delta\hat{\Phi}_{a,h} = \hat{\Phi}_a$ reduces to

$\Delta\hat{\Phi}_{a,h,D} = \hat{\Phi}_a$ and therefore to: $\left|\overset{\rangle}{N}_Q\left(\Omega_{e,\max}\right)\right| = \sqrt{2}\frac{\left|\overset{\rangle}{N}_D\right|}{SNR_{LOFI}}$ [see Eq. (16)].

By using the following approximation for the quantum noise: $\left|\overset{\rangle}{N}_Q\left(\Omega_{e,\max}\right)\right| \approx \sqrt{2}\sqrt{P_{out}}\frac{\gamma_c}{2\pi}\left|\frac{1}{F_{e,\max}}\right|\sqrt{\Delta F}$, one finally obtains:

$$F_{e,\max} = \frac{\Omega_{e,\max}}{2\pi} = \frac{\gamma_c}{2\pi} \times SNR_{LOFI} \frac{\sqrt{P_{out}\Delta F}}{\left|\overset{\rangle}{N}_D\right|} \quad \textbf{(18a)}$$

$$F_{a,\max} = F_{e,\max} - 1.1 \times F_R \quad \textbf{(18b)}$$

With the numerical conditions given in Eqs. (5a-d) and corresponding to the results shown in Figs. 2 and 3, one obtains: $F_{a,\max} \approx F_{e,\max} \approx 2GHz \approx 2000 \times F_R$, which is a quite high ultrasound frequency, despite the fact that the detection is made with a conventional detection, with a usual white noise level (thermal noise and quantization noise). One can also notice that the high value of $F_{e,\max}$ (and therefore of $F_{a,\max}$) principally comes from the use of a microchip laser with a high value of the laser cavity damping rate ($\gamma_c = 5 \times 10^9\,s^{-1}$). Let us recall that the high sensitivity of the LOFI setup to small reflectivities ($R_e << 1$) also comes from this high value of γ_c [16]. To summarize, Eq. (17a) gives: $\Delta\hat{\Phi}_{a,h,Q} \leq \Delta\hat{\Phi}_{a,h} \leq \sqrt{2}\Delta\hat{\Phi}_{a,h,Q}$ if $\hat{\Phi}_a = 10 \times \Delta\hat{\Phi}_{a,h,Q}$ and $0\,Hz \leq F_a \leq F_{a,\max}/10$. With the numerical conditions given in Eqs. (5a-d) one obtains: $\frac{\lambda}{9000} \approx 0.12\,nm \leq \Delta\hat{d}_{a,h} \leq 0.17\,nm \approx \frac{\lambda}{6000}$ for $\hat{d}_{a,h} = 1.2\,nm$ and $0\,Hz \leq F_a \leq 200\,MHz$, which corresponds to the following SNR range $10/\sqrt{2} \leq \hat{d}_{a,h}/\Delta\hat{d}_{a,h} \leq 10$ for the vibration amplitude. So even at high frequency the noise of the vibration amplitude keeps near the quantum limit given by Eq. (13).

Also Eqs. (13) and (10) shows that the sensitivity of the LOFI vibrometer can be increased (i.e. $\Delta\hat{d}_{a,h}$ decreases and $F_{a,\max}$ increases) if the laser output power and/or the effective reflectivity are increased. Average measurements and/or detection bandwidth reduction can also decrease the value of $\Delta\hat{d}_{a,h}$. In conclusion, the LOFI setup seems to be well adapted to measure, at high frequencies, the small amplitudes of harmonic vibrations of a target from which the back-reflected (or back-scattered) electric field is very weak $\left(R_e << 1\right)$.

B. Generic signal processing for vibrometry

In a more general situation where the vibration is not purely harmonic, but still in the specific case of small vibration amplitude: $d_a\left(t\right) << \lambda_c$, the time evolution of the phase induced by the vibration of the target ($\Phi_a\left(t\right)$) can be retrieved with the signal processing given by the following equation [12]:

$$\Phi_a(t) = 2\arg\left[\left[FT^{-1}\left[\frac{BPF(\Omega)FT[\Delta P_{out}(t)]}{G_R(\Omega)}\right]\right] \times \exp(-i\Omega_e t)\right]$$

(19a)

$$BPF(\Omega) = 1 \; for \; \Omega_e - \Delta\Omega_e \leq \Omega \leq \Omega_e;$$
$$BPF(\Omega) = 0 \; otherwise$$

(19b)

Firstly, the Fourier Transform (FT) of the time evolution of the laser output power is calculated. Secondly, this spectrum is filtered using a band-pass filter $BPF(\Omega)$ that only keeps the lower sideband (corresponding to the negative vibration frequencies) of the vibration spectrum located around the carrier frequency where the filter bandwidth $\Delta\Omega_e$ is adapted to the frequency range of the vibration spectrum. A typical value is $\Delta\Omega_e \approx \Delta\Omega_a$, where: $\Delta\Omega_a$ is the half width of the full vibration spectrum composed of both the negative and positive frequencies. As already explained, this specific filtering allows to keep the side of the vibration spectrum that is closest to the relaxation frequency and therefore with the lower relative noise. Thanks to this filtering, the noise of the LOFI vibrometer is minimized. Thirdly, the distortion of the vibration spectrum induced by the laser dynamics (i.e. the amplification gain $G_R(\Omega)$) is rectified. Back to the time domain, the signal is then demodulated (at the carrier frequency Ω_e) and finally, the time evolution of the target displacement is extracted by taking two times the argument of the complex signal. One can notice that the multiplicative factor 2 , in the beginning of Eq. (19a), allows to compensate for the loss of vibration energy induced by the band-pass filter, which only keeps the lower half of the vibration spectrum. This factor 2 corresponds to the one in Eqs. (9a-b) that comes from the approximation:

$$\Phi_a \approx 2J_1(\Phi_a)/J_0(\Phi_a) = -2J_{-1}(\Phi_a)/J_0(\Phi_a) \; .$$

Coming back temporarily to the specific case of a purely harmonic vibration and by using a band-pass filter with a bandwidth given by: $\Delta\Omega_e \approx \Omega_a$, one obtains:

$$BPF(\Omega) \times FT[\Delta P_{out}(t)] = 2\sqrt{R_e}\langle P_{out}\rangle$$
$$\times \left[\begin{array}{l} G_R(\Omega_e)J_0(\hat{\Phi}_a)\dfrac{\delta(\Omega-\Omega_e)}{2} + \\ G_R(\Omega_e-\Omega_a)J_{-1}(\hat{\Phi}_a)\exp(-j\varphi_a)\dfrac{\delta(\Omega-\Omega_e+\Omega_a)}{2} \end{array}\right]$$

(20a)

and therefore:

$$\left[\left[FT^{-1}\left[BPF(\Omega) \times FT[\Delta P_{out}(t)]/G_R(\Omega)\right]\right] \times \exp(-i\Omega_e t)\right]$$
$$\approx \frac{2\sqrt{R_e}\langle P_{out}\rangle}{2} \times \left[1 - \frac{\hat{\Phi}_a}{2}\exp(-j(\Omega_a t+\varphi_a))\right]$$

(20b)

And finally, for $\hat{\Phi}_a \ll 2\pi$, we can determine the time evolution of the target displacement by keeping the argument of the complex function given by Eq. (20b):

$$2\arg\left[\begin{array}{l}\left[FT^{-1}\left[\dfrac{BPF(\Omega) \times FT[\Delta P_{out}(t)]}{G_R(\Omega)}\right]\right]\\ \times \exp(-i\Omega_e t)\end{array}\right]$$
$$\approx \hat{\Phi}_a\left[\sin(\Omega_a t+\varphi_a)\right]$$

(20c)

In a more general situation where the vibration is not purely harmonic, its Fourier transform: $\Phi_a(t) = \int_{-\infty}^{+\infty}\hat{\Phi}_a(\Omega)\exp(-j\Omega t)d\Omega$ is simply a linear summation (over the frequency spectrum) of harmonic vibrations. Therefore, the signal processing given by Eqs. (19a-b) is generic and can be applied whatever the time evolution of the target displacement (harmonic or not).

C. Numerical study of transient vibration.

In order to verify that our signal processing can also be applied to the detection of non-harmonic vibrations with broad spectra, we have numerically simulated a laser with an optical reinjection coming from a target with a transient vibration (subscript τ):

$$\Phi_{a,\tau}(t) = \frac{\hat{\Phi}_{a,\tau}}{1+\left(\dfrac{t-\tau_d}{\Delta\tau_a}\right)^2}$$

(21)

Fig. 4 shows different RF power spectra of the laser intensity dynamics for a frequency shift of $F_e = 6.5 \times F_R$,a feedback reflectivity of the vibrating target of $R_e = 10^{-7}$ and for a transient vibration with a maximum amplitude $\hat{\Phi}_{a,\tau} = 2\pi/10$ ($\hat{d}_a = \lambda_c/20 \approx 50nm$), a half time width at half maximum $\Delta\tau_a \approx 0.05/F_R$ (i.e. a broad spectral bandwidth $\Delta F_a = \dfrac{1}{2\pi\Delta\tau_a} \approx 3 \times F_R$) and an arbitrary time delay $\tau_d = 52 \times \Delta\tau_a$. Without noise, Fig. 4(a) shows that the RF power spectrum is principally composed of a line at the modulation frequency (F_e). At the foot of this line, one can observe the broad vibration spectrum (with a half width ΔF_a) of the transient vibration:

$$FT[\Phi_a(t)] \otimes \delta(F-F_e) = \hat{\Phi}_a\pi\Delta\tau_a\left[\begin{array}{l}\exp\left[-\dfrac{|F-F_e|}{\Delta F_a}\right] \times \\ \exp\left[+j2\pi(F-F_e)\tau_d\right]\end{array}\right]$$

(22)

On can also observe a broad line at the relaxation frequency (F_R) not due to the noise, but due to the residue of the transient dynamic of the laser, and two small lines at $F_e \pm F_R$ induced by the nonlinear laser dynamics.
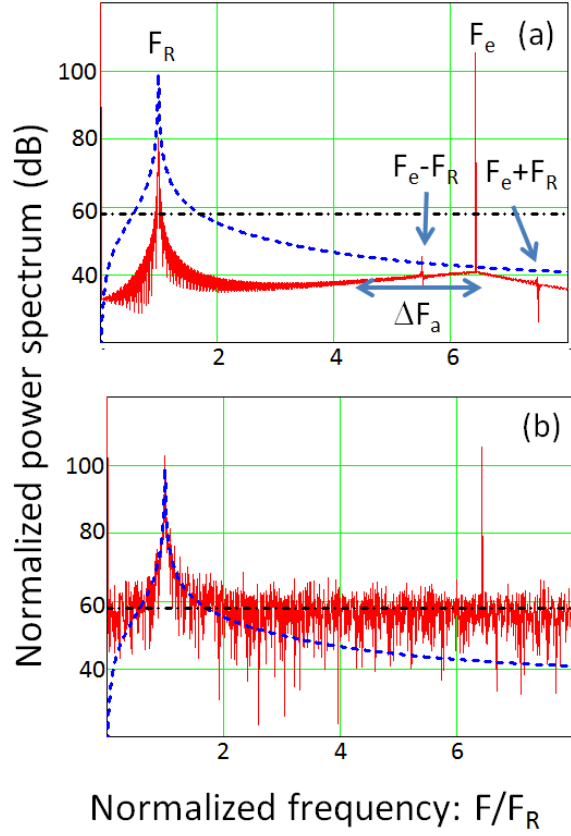
Fig. 4. Numerical simulations. Normalized power spectrum of the laser intensity dynamics. The normalization is made with the quantum shot-noise. a) Without noise, the broad line centered at the relaxation frequency (F_R) is a residue of the transient dynamic of the laser. b) With laser quantum noise and detector noise. The dashed curve is the theoretical laser quantum noise power spectrum. The horizontal dashed-dotted line is the mean value of the detection noise power spectrum. Optical feedback: $R_e = 10^{-7}$, $F_e = 6.5 \times F_R$. Transient vibration: $\hat{\Phi}_a = 2\pi/10$ (i.e. $\hat{d}_a = \lambda/20 = 53\,nm$), a full time width at half maximum $2\Delta\tau_a \approx 0.1/F_R \approx 100\,ns$ (i.e. a broad spectral bandwidth $\Delta F_a = \dfrac{1}{2\pi\Delta\tau_a} \approx 3 \times F_R \approx 3\,MHz$). The laser and detection parameters are given in Eqs. (5a-d).

When the detector noise and the laser quantum noise are added [Fig 4(b)], the vibration spectrum is completely drowned under the noise spectrum.

Although this situation seems unfavorable for the vibration detection, Fig. 5 shows that an accurate short transient vibration can be extracted from the RF power spectrum of the laser intensity dynamics by applying the signal processing given by Eqs. (19a-b). In the time domain, the vibration pulse is above the noise level ($\hat{\Phi}_{a,\tau} > \Delta\hat{\Phi}_{a,\tau}$), due to the coherent addition (during the inverse Fourier transform operation) of the spectral components of the vibration signal, while for the noise, the different spectral components add incoherently.

Also, Fig. 5 allows to compare the noise levels on the transient vibration (subscript τ) amplitude: $\Delta\hat{\Phi}_{a,\tau}$, obtained by using different band-pass filters in the signal processing given by Eqs. (19a-b).

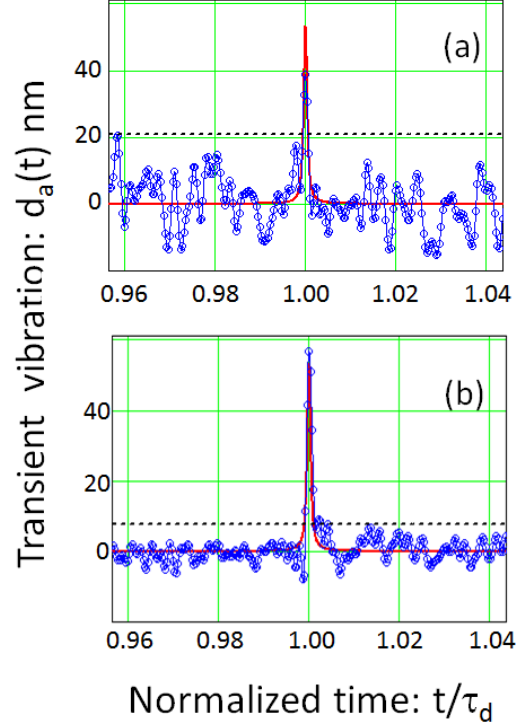Fig. 5. Numerical simulations. Detection of a transient vibration with a maximum amplitude: $\hat{d}_{a,\tau} = \lambda/20 = 53\,nm$ (i.e. $\hat{\Phi}_{a,\tau} = 2\pi/10$, with a full time width at half maximum: $2\Delta\tau_a \approx 0.1/F_R \approx 100\,ns$ and an arbitrary time delay: $\tau_d = 2.6/F_R \approx 2.6\,\mu s$) for two kinds of signal processing. Solid line: exact vibration motion. Circles: vibration obtained after the signal processing. The dashed horizontal line shows the noise level corresponding to 3 times the standard deviation (i.e. 99.7% probability) of the phase fluctuations. a) Full band-pass filtering. b) Partial band-pass filtering. In this case, the full vibration spectrum is reconstituted by the concatenation of 4 partial spectra obtained for 4 different frequency shifts. All the measurements are made with the same feedback reflectivity $R_e = 10^{-7}$. The laser and detection parameters are given in Eqs. (5a-d).

More precisely, to obtain the results shown in Fig. 5(a), the bandwidth of the filter is given by: $\Delta F_{e,1} = F_{max} - F_{min} = 5.4 \times F_R$ with $F_{max} = F_e = 6.5 \times F_R$ and $F_{min} = 1.1 \times F_R$. This RF filter with a large bandwidth ($\Delta F_{e,1} \approx 2 \times \Delta F_a$) allows to keep 97 % of the energy of the lower sideband of the vibration spectrum. As we can see, this adapted filter allows to restore the good shape of the transient vibration. One can notice that if $\Delta F_{e,1}$ is larger, the noise increases without any significant improvement of the reconstructed pulse shape while if $\Delta F_{e,1}$ is smaller, the noise decreases, but the strongest truncation of vibration spectrum induces a deterioration of both the amplitude and the duration of the reconstructed transient vibration.

In the simulations of Fig. 5, the numerical noise level $\Delta\hat{\Phi}_{a,\tau}$ is obtained by calculating the standard deviation of the phase fluctuations measured outside the time domain of the transient vibration.

In Fig. (5a), the measured phase noise is equal to: $\Delta\hat{\Phi}_{a,\tau,1} = 0.082\,rad$ (i.e. $\Delta\hat{d}_{a,\tau,1} = 6.7\,nm$) in agreement with $\Delta\hat{\Phi}_{a,\tau,1} = \sqrt{\Delta\hat{\Phi}_{a,\tau,Q}^2 + \Delta\hat{\Phi}_{a,\tau,D}^2} = 0.086\,rad$ where, for a transient vibration, the phase noise induced by the laser quantum noise and the detection noise are respectively given by:

$$\Delta\hat{\Phi}_{a,\tau,Q} = \sqrt{\int_{F_e - \Delta F_e}^{F_e} \frac{\Delta\hat{\Phi}_{a,h,Q}^2}{\Delta F}\,dF}$$

$$\approx \frac{2\sqrt{2}}{SNR_{LOFI}}\sqrt{\frac{\Delta F_e}{\Delta F}} = 0.038\,rad$$ (23a)

$$\Delta\hat{\Phi}_{a,\tau,D} = \sqrt{\int_{F_e - \Delta F_e}^{F_e} \frac{\Delta\hat{\Phi}_{a,h,D}^2}{\Delta F}\,dF}$$

$$\approx \Phi_a \sqrt{2}\,\frac{F_e}{F_{e,\max}}\,\frac{\sqrt{\Delta F_e}}{\sqrt{\Delta F}} = 0.077\,rad$$ (23b)

The result shown in Fig. 5(b) has been obtained with bandpass filter narrower than the previous one: $\Delta F_{e,4} = F_{\max} - F_{\min} = 1.35 \times F_R = \Delta F_d\,/4$, but with the same value of $F_{\min} = 1.1 \times F_R$, and therefore a smaller value of $F_{\max} = 2.45 \times F_R$. With this filter, to restore the good shape of the transient vibration, the full vibration spectrum has been reconstituted by the concatenation of 4 partial spectra obtained with the same bandpass filtering near the relaxation frequency, but with 4 different values of the frequency shift: $F_{e,n} = \left[2.45 + (n-1) \times 1.35 \right] \times F_R$ with $n \in [1,2,3,4]$.

One can notice that the width of the filter and its central position haven't be chosen arbitrarily, but have been optimized in order to minimize the phase noise (i.e. to minimize the effect of the detection noise) of the restored vibration with the minimum number of partial spectra. For the laser and detection parameters given by Eqs; (5a-d) this number is equal to: 4. Indeed, by using this optimized protocol, one can see in Fig. 5(b), that we are able to retrieve the good shape for the transient vibration with a noise ($\Delta\hat{\Phi}_{a,\tau,4} = 0.040\,rad \approx \Delta\hat{\Phi}_{a,\tau,Q}$) at the laser quantum noise level [see Eq. 23(a)].

One can also notice, the vibration shape could also have been restored by the concatenation of a larger number ($n > 4$) of narrower partial spectra, but, when the number of partial spectra is increased, the concatenation method becomes less and interesting by comparison with an averaging of n measurements obtain with the initial filter (with the full width $\Delta F_{e,1} = 5.4 \times F_R$).

The conclusion of this section is that whatever the width of the vibration spectrum (i.e. whatever the duration of the transient vibration), its seems that we are always able to restore the shape of a transient vibration at the shot noise level by acquiring the vibration spectrum part by part, in the vicinity of the laser relaxation frequency. This protocol seems to be particularly interesting in the case of detection noise that can't be reduced by averaged measurements.

D. Experimental study of transient-harmonic vibrations

With a LOFI setup (Fig. 1), we have experimentally measured the transient-harmonic vibrations of the air/water interface of our tank. The laser is set to an output power of $10\,mW$ with a relaxation frequency of $F_R = 1.3\,MHz$ and the carrier frequency (controlled by two AODs) is tuned to $F_e = 11.6\,MHz$ (i.e. $\approx 9 \times F_R$). Experimentally, the observed LOFI SNR is equal to $SNR_{LOFI} = 1298$, corresponding to a weak effective feedback reflectivity of $R_e \approx 4 \times 10^{-8}$ (controlled by playing with the efficiency of the two AODs).

The transient-harmonic vibration of the air/water interface is generated by an immersion ultrasound transducer (NDT Systems, IBMF104, $F_a = 10\,MHz$). The transducer, with a diameter of 13 mm and a focal length of 26 mm, is immerged inside a tank filled with water and the depth ($\approx 3\,cm$) of the transducer is aligned in that way, that its focus lays near to the air/water interface in order to generate significant perturbations in the surface of the fluid.

The transducer is used in a "burst mode", where the applied voltage is composed of 100 harmonic oscillations at a frequency of $F_a = 10\,MHz$. Experimentally, the vibration of duration $\Delta\tau_a = 10\,\mu s$ (i.e. $\Delta F_a = 100\,kHz$)) is triggered after a time delay of $310\,\mu s$. The total recording time is $T = 1.31\,ms$ (i.e. $\Delta F = 1/T = 763\,Hz$) with a sampling rate of $1 \times 10^8\,samples/s$ (DAQ card: SPECTRUM/ M3I.4111).

The applied voltage on the transducer has a rms amplitude of $33V$, obtained from the association of a function generator (Agilent 33250A) with an output rms amplitude of $100\,mV$ and a RF amplifier (E&I/325LA) with a power gain of $50\,dB$. Under this condition, the delivered power is equal to the nominal power of the RF amplifier (i.e. $25W$) and due to the duty cycle ($10\,\mu s/1.31\,ms$) the mean power applied to the PZT is relatively high : $180\,mW$ (i.e. near the damage threshold).

Under these conditions, the overpressure generated at the acoustic focus point (i.e. near the air/water interface) is high and equals to: $\hat{p}_{a,\exp}$; $700\,kPa$. Experimentally, this overpressure has been measured by using a hydrophone (DAPCO Industries), roughly calibrated ($\approx 5V/MPa\,@\,2MHz$).

Theoretically, this overpressure allows to generate a transient-harmonic displacement of the water surface with an amplitude of: $\hat{d}_{a,th} = \frac{2\hat{p}_{a,\exp}}{Z_{eau}\,2\pi F_a} \approx 15\,nm$, where $Z_{eau} = 1.5 \times 10^6\,Pa\,s\,m^{-1}$ is the acoustic impedance of water [24].

Fig. 6 shows that quantitative vibration measurements can be experimentally extracted from the laser dynamics with a LOFI setup. Indeed, the averaged value of measured vibration amplitude is equal to: $\hat{d}_{a,\exp} \approx 24\,nm \pm 5\,nm$ (Fig 5a) or $\hat{d}_{a,\exp} \approx 21\,nm \pm 2\,nm$ (Fig 5b), in relatively good agreement with our "linear" theoretical

prediction $\hat{d}_{a,th} \approx 15\,nm$ and this, even if the generated acoustic overpressure pressure is very important.

The time delay ($\approx 20\,\mu s$) between the time gates when the ultrasonic transducer is triggered and when the ultrasonic vibration is detected is due to the transit time of the acoustic wave in water with a velocity: $\approx 1490\,m/s$ (room temperature) and a propagating distance of $\approx 3\,cm$. It should be noted that each presented time trace is an average of 10 acquisitions.

The measurements shown on Figs. 6(a and b), have been obtained with a selective band-pass filter:

$$\begin{aligned} BPF(F) &= 1 \ for \ F = F_e \\ BPF(F) &= 1 \ for \ F_a - \Delta F_e/2 \leq F \leq F_a + \Delta F_e/2 \\ BPF(F) &= 0 \ otherwise \end{aligned} \quad \textbf{(24)}$$

where $\Delta F_e = 8 \times \Delta F_a$ for the result in Fig. 6(a) and $\Delta F_e = 1 \times \Delta F_a$ for Fig. 6(b).

When the width of the band-pass filter decreases, one can also observe how the truncation of the vibration spectrum deteriorates the rectangular shape of the vibration envelope. One can also observe how the experimental (subscript exp) phase noise decreases: $\Delta\hat{\Phi}_{a,\exp} = 0.059\,rad$ ($\Delta\hat{d}_{a,\exp} = 5\,nm$) and $\Delta\hat{\Phi}_{a,\exp} = 0.021\,rad$ ($\Delta d_{a,\exp} = 1.78\,nm$) proportionally to $\sqrt{\Delta F_e}$.

According to us, the last case [Fig. 6(b)] is a good compromise. Indeed, although the shape of the reconstructed vibration envelope is not good (not a rectangular temporal gate), this filtering allows to roughly determine the maximum of the vibration amplitude, the duration of the time gate (by measuring the full width at half maximum of the reconstructed vibration) and to minimize the phase noise. Regarding this last point, the measured value is in perfect agreement with the theoretical prediction given by Eq. (25) for a ten times averaged measurement:

$$\begin{aligned} \Delta\hat{\Phi}_{a,\exp} &= \frac{1}{\sqrt{10}} \sqrt{\int_{F_a - \Delta F_e/2}^{F_a + \Delta F_e/2} \frac{\Delta\hat{\Phi}_{a,h,Q}^2}{\Delta F} dF} \\ &\approx \frac{1}{\sqrt{10}} \frac{2\sqrt{2}}{SNR_{LOFI}} \sqrt{\frac{\Delta F_e}{\Delta F}} = 0.021\,rad \end{aligned} \quad \textbf{(25)}$$

This simple experiment example confirms that the LOFI setup is adapted to detect at ultrasound frequency ($F_a = 10\,MHz$) the small amplitudes ($2 \times \Delta\hat{d}_{a,\exp} \approx 4\,nm$) of short vibrations ($\Delta\tau_a = 10\,\mu s$) of a target with a weak feedback reflectivity ($R_e \approx 4 \times 10^{-8}$).

4. CONCLUSION AND PERSPECTIVES

In this paper, we have demonstrated the possibility to accurately measure very small vibration amplitudes in the ultrasound domain by using a LOFI setup with a low power laser and a conventional photodiode and that the smallest vibration amplitude which can be detected is shot noise limited and is given by:

$$\hat{d}_{a,\lim} = \frac{1}{\sqrt{N}} \frac{\lambda}{2\pi} \frac{\sqrt{2\Delta F_e}}{\sqrt{R_e P_{out}}} \quad \textbf{(26)}$$
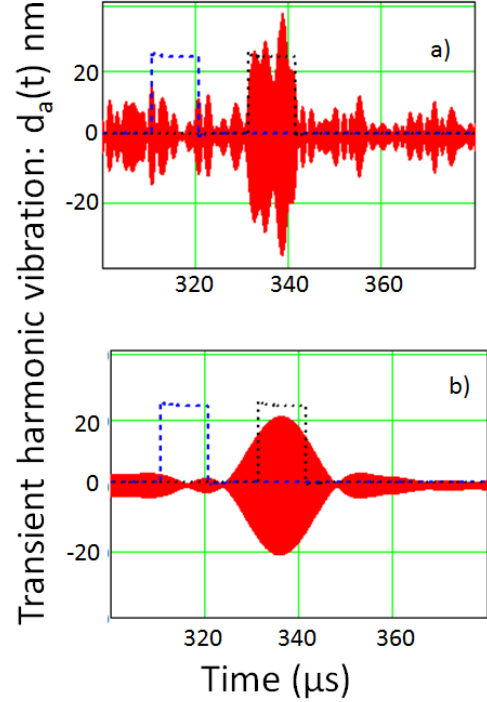
where is N the number of averaged measurements.

Fig.. 6. Experimental results. Detection on the water surface of a transient-harmonic vibration generated by an ultrasonic transducer located $\approx 3\,cm$ below the air/water interface. Oscillation frequency: $F_a = 10\,MHz$, vibration duration: $\Delta\tau_a = 10\,\mu s$. The measurement is made for $F_e = 11.6\,MHz$ and the signals are extracted from different bandwidth filters: a) $\Delta F_e = 8/\Delta\tau_a = 0.8\,MHz$; vibration amplitude: $d_a \approx 24\,nm \pm 5\,nm$, b) $\Delta F_e = 1/\Delta\tau_a = 0.1\,MHz$; vibration amplitude: $d_a \approx 21\,nm \pm 2\,nm$. Full line: the vibrations extracted by the signal processing; Dashed curve: the time gate when the ultrasonic transducer is triggered; Dotted curves: the time gate when the ultrasonic vibrations need to appear due to the transit time of sound in water.

More precisely, we have shown that for a harmonic vibration with an amplitude in the nanometer range, the amplitude of the laser intensity modulation at the carrier frequency is several order of magnitude higher than the amplitude of the vibration sidebands induced by the acoustic frequency. Nevertheless, the lower vibration sideband, which has a small amplitude, can be detected if it is located near the laser relaxation frequency, where the LOFI detection is shot-noise limited. By using this method, we have theoretically demonstrated that an acoustic frequency of the order of several GHz can be detected with a LOFI setup, even if a conventional detection, with a usual noise level is used to detect the laser intensity modulation. Let us recall that the high sensitivity of the LOFI setup for the detection of high acoustic frequencies comes from the use of a microchip laser with a small cavity length and therefore with a high value of the laser cavity damping rate.

For a transient vibration, we have also shown that it is possible to reconstruct the temporal shape of the vibration by acquiring the vibration spectrum part by part, through a band-pass filter that selects the frequencies in the vicinity of the laser relaxation frequency. This protocol allows to realize phase measurements with very low noise

(i.e. at the laser quantum noise limit), even if the detection has a high noise level. From our numerical study, we can conclude that the LOFI setup seems to be well adapted to detect high vibration frequencies (or broad vibration spectra), up to the ultra-high frequency domain, with subwavelength amplitudes on surfaces with a very weak feedback reflectivity.

Finally, we have experimentally detected (at the air/water interface) transient-harmonic vibrations with nanometer amplitude, generated by an ultrasonic transducer with a central acoustic frequency of 10 MHz, immersed 3 cm below the water surface. These conditions correspond to the detection at the surface of a biological tissue of an ultrasound vibration generated by a photoacoustic effect in an absorbing blood vessel with a characteristic diameter of 50-100 μm [25-27]. The use of a LOFI setup for the optical detection of photoacoustic signals is currently in progress.

References

1. R. Lang and K. Kobayashi, "External optical feedback effects on semiconductor injection laser properties ," IEEE J. Quantum Electron. **QE-16**, 347-355 (1980).

2. T. Erneux, V. Kovanics, and A. Gavrielides, "Non-linear dynamics of an injected quantum cascade laser," Phys. Rev. E **88**, 032907 (2013).

3. T. Taimre, M. Nikolic, K. Bertling, Y. L. Lim, T. Bosch and A. D. Rakic,"Laser feedback interferometry: a tutorial on the self-mixing effect for coherent sensing," Adv. in Opt. and Photon. **7**, 570,631 (2015)

4. S. Okamoto, H. Takeda, and F. Kannari, "Ultrahighly sensitive laser-Doppler velocity meter with a diode-pumped Nd:YVO4 microchip laser," Rev. Sci. Instrum. **66,** 3116–3120 (1995).

5. K. Otsuka, "Effects of external perturbations on $LiNdP_4O_{12}$ Lasers," IEEE J. Quantum Electron., **QE-15**, 655-663 (1979).

6. K. Otsuka, "Self-Mixing Thin-Slice Solids-State Laser Metrology," Sensors **11**, 2195-2245 (2011).

7. Y. Tan, S. Zhang, S. Zhang, Y. Zhang and N. Liu, "Response of microchip solid state laser to external frequency-shifted feedback and its applications," Sci. Rep. **3**, 2912 (2013).

8. R. Kawai, Y. Asakawa, K. Otsuka, "Ultrahigh-Sensitivity Self-Mixing Laser Doppler Velocimetry with Laser-Diode-Pumped Microchip $LiNdP_4O_{12}$ Lasers," IEEE Photonics Technology Lett. **11**, 706-708 (1999).

9. S. Suddo, T. Ohtomo, Y. Takahascvhi, T. Oishi, K. Otsuka, "Determination of velocity of self-mobile phytoplankton using a self thin-slice solid–state laser," Appl. Opt. **48**, 4049-4055 (2009).

10. K. Otsuka, K. Abe, J.Y. Ko, and T.S. Lim, "Real-time nanometer vibration measurement with self-mixing microchip solid-state laser," Opt. Lett. **27**, 1339-1341 (2002).

11. V. Muzet, E.Lacot, O. Hugon, Y. Gaillard, "Experimental comparison of shearography and laser optical feedback imaging for crack detection in concrete structures," Proc. SPIE 5856, 793-799 (2005).

12. V. Giradeau, C. Goloni, O. Jacquin, O. Hugon, M. Inglebert, E. Lacot, "Nonlinear laser dynamics induced by frequency shifted optical feedback : application to vibration measurements," Appl. Opt. **55**, 4049-4055 (2016).

13. E. Lacot, R. Day, and F. Stoeckel, "Laser optical feedback tomography," Opt. Lett. **24,** 744–746 (1999).

14. O. Hugon, F. Joud, E. Lacot, O. Jacquin, H. Guillet de Chatellus, "Coherent microscopy by laser optical feedback imaging (LOFI) technique," Ultramicroscopy (2011) doi: 10.1016/j.ultramic.2011.08.004.

15. W. Glastre, O. Hugon, O. Jacquin, H. Guillet de CHatellus, and E. Lacot, "Demonstration of a plenoptic microscope based on laser optical feedback imaging," Opt. Exp. **21**, 7294–7303 (2013).

16. E. Lacot, R. Day, "Coherent laser detection by frequency-shifted optical feedback," Phys. Rev. A **64**, 043815 (2001).

17. E. Lacot, O. Jacquin, G. Roussely, O. Hugon, H. Guillet de Chatellus, "Comparative study of autodyne and heterodyne laser interferometry for imaging," J. Opt. Soc. Am. A **27**, 2450-2458 (2010).

18. O. Jacquin, E. Lacot, W. Glastre, O. Hugon, H. Guillet de Chatellus, "Experimental comparison of autodyne and heterodyne laser interferometry using an Nd:YVO4 microchip laser," J. Opt. Soc. Am. A **28**, 1741-1746 (2011).

19. K. Bertling, J. Perchaoux, T. Taimre, R. Malkin, D. Robert, A. D. Rakic, and T. Bosch, "Imaging of acoustic fields using optical feedback interferometry," Opt. Exp. **22**, 30346-30356 (2014).

20. F. J. Azcona, R. Atashkhooei, S. Royo, J. Mendez Astudillo, and A. Jha, "A Nanometric Displacement Measurement System Using Differential Optical Feedback Interferometry," IEEE Photoncis Technology Lett. **25** 2074-2077 (2013).

21. K. Peterman, Laser diode modulation and noise (Springer, 1988)

22. M.I. Kolobov, L. Davidovitch, E. Giacobino, and C. Fabre, "Role of pumping statistics and dynamics of atomic polarization in quantum fluctuations of laser sources," Phys. Rev. A **47**, 1431-1446 (1993).

23. E. Lacot, O. Hugon, "Phase-sensitive laser detection by frequency-shifted optical feedback," Phys. Rev. A **70**, 053824 (2004).

24. J. Horstmann, H. Spahr, C. Buj, M. Munter, and R. Brinkmann, "Full-Field speckle interferometry for non-contact photoacoustic tomography," Phys. Med. Biol. **60**, 4045-4058 (2015)

25. C. Li and L.V. Wang, "Photoacoustic tomography and sensing in biomedicine," Phys. Med. Biol. **54**, R54-R97 (2009).

26. S. A. Carp and V. Venugopalan,"Optoacoustic imaging based on the interferometric measurement of surface displacement," J. of Biomed. Opt. **12**, 064001 (2007).

27. B. Dong, C. Sun and H. F. Zhang, "Optical detection of ultrasound in photoacoustic imaging," IEEE Trans. Biomed. Engi. **54**, 4-15 (2017).